Response of Cells on Surface-Induced Nanopatterns: Fibroblasts and Mesenchymal Progenitor Cells

Hwei Ling Khor,*,† Yujun Kuan,‡ Hildegard Kukula,§ Kaoru Tamada,|| Wolfgang Knoll,†,§ Martin Moeller,# and Dietmar W. Hutmacher*,⊥,&

Max-Planck Institute for Polymer Research, 10 Ackermannweg, 55128 Mainz, Germany, Department of Mechanical Engineering, National University of Singapore, 9 Engineering Drive 1, 117576 Singapore, Department of Chemistry and Materials Science, National University of Singapore, 10 Science Drive 4, 117543 Singapore, Department of Electronic Chemistry, Interdisciplinary Graduate School of Science and Engineering, Tokyo Institute of Technology, Nagatsuta, Yokohama 226-8502, Japan, Organische Chemie III-Makromolekulare Chemie, Universität Ulm, Albert Einstein Allee 11, D-89081 Ulm, Germany, Division of Bioengineering, Faculty of Engineering, National University of Singapore, 7 Engineering Drive 1, 117574 Singapore, and Department of Orthopaedic Surgery, Faculty of Medicine, National University of Medicine, Lower Kent Ridge Road, 119074 Singapore

Received December 4, 2006; Revised Manuscript Received February 8, 2007

Ultrathin films of a poly(styrene)-*block*-poly(2-vinylpyrindine) diblock copolymer (PS-*b*-P2VP) and poly(styrene)-*block*-poly(4-vinylpyrindine) diblock copolymer (PS-*b*-P4VP) were used to form surface-induced nanopattern (SINPAT) on mica. Surface interaction controlled microphase separation led to the formation of chemically heterogeneous surface nanopatterns on dry ultrathin films. Two distinct nanopatterned surfaces, namely, wormlike and dotlike patterns, were used to investigate the influence of topography in the nanometer range on cell adhesion, proliferation, and migration. Atomic force microscopy was used to confirm that SINPAT was stable under cell culture conditions. Fibroblasts and mesenchymal progenitor cells were cultured on the nanopatterned surfaces. Phase contrast and confocal laser microscopy showed that fibroblasts and mesenchymal progenitor cells preferred the densely spaced wormlike patterns. Atomic force microscopy showed that the cells remodelled the extracellular matrix differently as they migrate over the two distinctly different nanopatterns.

Introduction

Cells generally attach to artificial culture substrata by binding to specific proteins that are adsorbed to the surface of the substrate. The best characterized attachment molecules are components of the extracellular matrix (ECM), such as fibronectin (FN), laminin, proteoglycans, elastin, and different collagens, that form a three-dimensional scaffolding which supports cell anchorage in vivo. The adhesion-supporting activity of serum, usually present in cell culture media, is now thought to be largely due to two ECM proteins, FN, and vitronectin that are normally found in serum.[1]

In vivo, many cells adhere to extracellular matrices which have a complex 3D topography in the micrometer-to-nanometer range.[2] In addition, micro- and nanoscale mechanical stresses generated by cell-matrix adhesion have a significant effect on cellular phenotypic behavior. The structural organization of tissue plays a major part in deciding the degree and direction of tissue growth and cell movement, and the effect had been termed contact guidance.[2]

To develop the next generation of medical devices and implants, the ability to control the attachment, proliferation, and differentiation of cells will be highly desirable. Knowledge of substrate−cell interaction is important to avoid the formation of fibrous capsules that form around a great number of the currently applied prosthesis. The effects of microtopography on cell adhesion, contact guidance, and cytoskeleton organization had been studied extensively.[3,4]

Clark et al.[5,6] and Wojciak-Stothard et al.[7] have shown that cell adhesion is complex varying with cell types as well as with the nature of the surface. Grooves are the most common features employed to investigate surface topography effects on cells.[5,8,9] There is general evidence that the extent of orientation increases with groove depth up to 25 μm from topographies of about 1-μm relief.

Evidence is now gathering on the importance of nanoscale dimensions in the design of biomaterials used in tissue engineering applications too.[4,9−14] Wojciak-Stothard and co-workers[7,15] discovered that P288D1 macrophage-like cells react down to dimensions at least as small as 44 nm. Epithelia, fibroblasts, and endothelia cells could react to depths as shallow as 70 nm.[3] Such small topographies approach the dimensions of large molecules and give rise to suspicions that the sensing mechanisms of cells for topography are perhaps as sensitive as those of the atomic force microscope.

Spatz and co-workers[16−18] reported that ultrathin films of a symmetrical polystyrene-*block*-poly(2-vinylpyridine) diblock copolymer assemble on mica to form heterogeneous surface patterns. The films have been prepared in such a way that the average thickness of the polymer is much less than the

* Authors to whom correspondence should be addressed. E-mail: (H.L.K.) khor@mpip-mainz.mpg.de; (D.W.H.) biedwh@nus.edu.sg.
† Max-Planck Institute for Polymer Research.
‡ Department of Mechanical Engineering, National University of Singapore.
§ Department of Chemistry and Materials Science, National University of Singapore.
|| Tokyo Institute of Technology.
Universität Ulm.
⊥ Faculty of Engineering, National University of Singapore.
& Department of Orthopaedic Surgery.

10.1021/bm0611533 CCC: $37.00 © 2007 American Chemical Society
Published on Web 03/28/2007

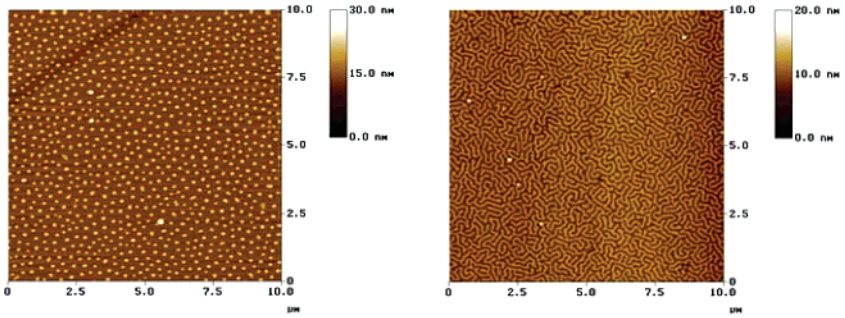

Figure 1. AFM images of $PS_{1350}P2VP_{400}$ and $PS_{610}P4VP_{130}$ substrates with dotlike and wormlike nanopatterns, respectively.

equilibrium period of the bulk morphology. Strongly adsorbed P2VP blocks wet the mica surface as an ultrathin, 1−3 nm thick polymer layer that has a largely extended chain formation. By using the nanoscale architectural control of this technique, this work examines how different nanopatterns control and influence cell adhesion and proliferation of human-derived dermal fibroblasts and mesenchymal precursor cells.

Materials and Methods

Substrate Preparation. Diblock copolymers of polystyrene-*block*-poly(2-vinylpyridine) with different block lengths (Figure 1) were dissolved in a nonselective solvent, chloroform, at a stock concentration of 0.4 mg/mL. The diblock copolymers were synthesized and kindly supplied by Prof. M. Moeller from the University of Ulm, Germany. The working polymer solution was diluted 10 times to give a final polymer concentration of 0.04 mg/mL. Freshly cleaved mica (ASTM V-1 Quality Ruby Mica, size 10 × 20 mm, thickness 0.3 mm, Microfab, India) substrates were dip-coated with the dilute polymer solution for 30 s and were pulled out at a constant velocity of 10 mm/min. The polymer films were annealed at 140 °C for 2−3 h under vacuum in a vacuum oven (B Braun, Melsungen, Germany). The working polymer solution was freshly prepared before dip coating and the coated samples were stored in a humidity cabinet (20−30% humidity) until tested.

Atomic Force Microscopy (AFM). Topography was scanned with an atomic force microscope (Nanoscope Dimensions 3100, Digital Instruments, New York) in the tapping mode. Tips of spring constant 47 N/m (Crest Technology, Singapore) were used. Each substrate was mounted on an aluminum specimen holder with double-sided carbon tape for viewing.

Substrate surfaces were also scanned in contact mode in liquid to determine effects of serum absorption to the nanopatterns. Tips of spring constant 0.12 N/m were used in this case. Prior to atomic force microscopy, two sets of dotlike and wormlike nanopattern substrates were incubated with cell culture medium in a humidified 37 °C/5% CO_2 atm incubator for 2 h. Culture medium used was Dulbeccos Modified Eagles Medium (Gibco, NY) supplemented with 0.5% or 10% concentration fetal bovine serum (Hyclone, UT) respectively. To maintain good visibility of substrate nanopatterns during the AFM measurements, the culture medium which contains phenol red was replaced by phosphate-buffered saline (Gibco, NY) with 0.5% or 10% concentration of fetal bovine serum (FBS). Surface roughness values of the substrates were measured in a 5 μm × 5 μm area. Cross section analysis was done with the AFM data (5 μm × 5 μm area) of the samples in triplicates to measure the topography of the nanostructures. The area of the surfaces covered by the polystyrene domains was calculated by converting the AFM images into gray scale images and a free picture editing software, ImageJ 1.37h, was used to calculate the area.

Contact Angle Measurements. Contact angle measurements of the substrates were monitored before and after sterilization with 70% ethanol and after 2 h incubation at 37 °C with cell culture media supplemented with low fetal bovine serum content (0.5%) and normal fetal bovine serum content (10%). Substrates incubated with cell culture media were rinsed once with deionized water and were dried before contact angle measurements.

Surface energy determinations of different nanopatterned substrates were performed by water contact angle measurement analysis using the VCA Optima machine (Advance Surface Technology, MA). The sessile drop is slowly grown to a radius of approximately 5 mm and is dropped onto the substrate surface. The droplet is allowed to stabilize for 1 min before measurements of contact angles are taken. By repeatedly adding small amounts of liquid to the drop and advancing it over fresh areas of the solid, many contact angles can be measured to give an average representation of a relatively large area of the surface.

Cell Culture Study. Two types of cells, fibroblasts and mesenchymal precursor cells (MPC), were cultured on the substrates. Cells were obtained with consent from patients undergoing routine surgery according to the ethical guidelines of the Helsinki II declaration and as approved by the National University of Singapore Institutional Review Board. All media, supplements, and chemicals were purchased from Gibco (Invitrogen Corp, Grand Island, NY) unless otherwise stated in the text. Fibroblasts and MPCs were cultured in Dulbecco's Modified Eagle Medium (DMEM) with 10% FBS. All cell culture media were supplemented with 1% penicillin-streptomycin. Prior to cell seeding, 80% confluent cultures were enzymatically lifted from T75 cell culture flasks with 0.05% trypsin-EDTA (Hyclone, UT) and were counted with a hemocytometer. Cell viability was assessed with Trypan blue staining.

Coated mica substrates were examined under atomic force microscopy before being selected for cell culture study to ensure that the surfaces were coated with the nanopatterns. Prior to seeding the cells on the substrates, all substrates were cut into 10 mm × 10 mm pieces and were sterilized by gently washing in 70% ethanol for less than 5 min and left to dry. Fibroblasts and MPCs were seeded at a low cell density of 1.0×10^4 cells/cm^2. The seeded specimens were then left for 4 h in the incubator at 37 °C and 5% CO_2 for cell attachment to occur. The samples were then carefully topped with 2 mL of culture media, and constructs were kept in culture for up to 10 days. Cells were seeded on eight replicates of each of the distinct topographies created.

Phase Contrast Light Microscopy. The study of cell morphology, intercellular connections, and qualitative cell proliferation over time were examined daily by phase-contrast light microscopy (Leica DM IRB, Germany) up to 7 days in vitro. Images of two different regions of each substrate were taken at day 1, 4, and 7.

Confocal Laser Microscopy. To view the actin cytoskeleton of the cells on the substrates after 7 days in vitro, they were first fixed in 3.7% formaldehyde (Merck, Darmstadt, Germany) at room temperature for 30 min. After rinsing twice with PBS for 5 min each time, 200 μg/mL RNAse A was added and left for 30 min at room temperature. Phalloidin (A12379 Alexa Fluo 488 Phalloidin, Molecular Probes Inc., OR) was then added at a 1:200 dilution, and the samples were incubated in the dark for 45 min at room temperature. The samples were subsequently counterstained with 5 μg/mL propidium iodide (PI) solution which stains the nucleus red. The samples were then dried

Table 1. Physical Properties of the Nanopatterns Generated on DS1 and LS1 Substrates[b]

PS-b-P2VP 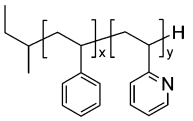 PS-b-P4VP 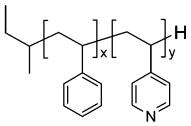

sample	di-block copolymer	N_{PS}/N_{VP}[a]	*h* (nm)	Ra (nm)	*W* (nm)	c−c (nm)	% PS
DS1	PS(1350)-*b*-P2VP(400)	3.38	6.0 ± 0.5	0.47 ± 0.07	200 ± 10	290 ± 20	21.3 ± 1.5
LS1	PS(610)-*b*-P 4VP(130)	4.69	3.2 ± 0.2	0.17 ± 0.02	160 ± 7		61.1 ± 1.9

[a] N_{PS}/N_{VP} = ratio of length of PS block to length to PVP block, *h* = average height of nanopatterns, Ra = surface roughness of substrates, *W* = width of nanopatterns, c−c = center to center distance of nanopatterns, % PS = percentage area of substrate covered by the polystyrene domains. [b] The chemical structures of the block copolymers are shown above the table.

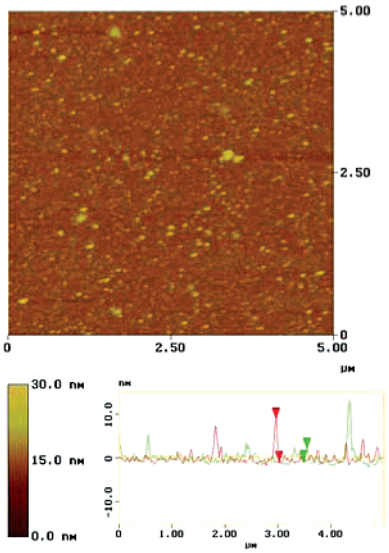

Figure 2. AFM image of uncoated mica substrates after 2 h incubation with medium that is supplemented with 10% FBS. (The cross-sectional profile of the substrate along a straight line picked at random is shown at the bottom right.)

and mounted for viewing under a Confocal Laser Microscope (Olympus IX70-HLSH100 Fluoview, PA). Images were taken from four different regions of one sample from each of the two groups of substrates. Images were taken at magnification of 10×, 20×, 40×, and 60× objective.

MPC were transfected with eYFP-α-tubulin plasmid (Cat: 6118−1, Clontech, CA). The cells were electroporated (Nucleofector, Amaxa Biosystems, Cologne, Germany) according to manufacturer's instruction. The procedure is described briefly here. The cells were trypsinised and resuspended in Nucleofactor solution provided by Amaxa Biosystems at 4−5 × 10^5 cells/100 μL. One hundred microliters of cell suspension was mixed with 2−3 μg of DNA and was transferred to an Amaxa certified cuvette. A preprogrammed electroporation condition (C-17) was selected to give the highest cell survival. Cells were transferred immediately to six prepared well plates containing prewarmed cell culture media. Cells were cultured for 48 h after electroporation to achieve maximum YFP expression. The cells were then again trypsinized and sorted using a flow cytometer (BD FACSVantage SE System, BD Biosciences, CA). The fluorescence excitation and emission maximum of eYFP is 513 and 527 nm. The sorted cells were seeded on the surface-induced nanopattern (SINPAT) substrates in triplicates, and images were taken at three different regions of each sample at a magnification of 60× objective with a confocal laser microscope (Olympus IX70-HLSH100 Fluoview, PA).

Atomic Force Microscopy. MPC cultures on DS1 and LS1 substrates after 7 days in vitro were fixed by freeze-drying with liquid nitrogen in a freeze dryer (Heto, Lyolab 3000). The samples were then examined under AFM in the tapping mode as described before.

Results

Substrate Fabrication and Characterization. As reported by Spatz and co-workers, poly(styrene)-*block*-polyvinylpyridine (PS-*b*-PVP) diblock copolymer on mica can form a chemically heterogeneous surface pattern.[16−20] The ultradilute concentration of the diblock copolymer dissolved in a nonselective solvent (0.04 mg/mL) and the strong preferential adsorption of one of the blocks lead to the microphase separation and self-ordering of the ultrathin block copolymer film. Strong interactions between the PVP chains and mica cause the PVP block to adsorb as a quasi two-dimensional layer whereas the PS chains aggregate on top of the PVP layer into three-dimensional dewetting structures. It has been demonstrated that the aggregates are separated from the mica surface by only a 1-nm-thick layer of P2VP chains that are tightly adsorbed to the mica surface.[16,18] PS-*b*-P2VP polymers preferably form dotlike morphologies while wormlike morphologies are obtained only from PS-*b*-P4VP block copolymers. The size and morphology of the surface-induced nanopatterns (SINPAT) on mica depend essentially on the relative length of the blocks. Experimental results about the effects of variation of block length on the size and morphology of the nanopatterns have been reported elsewhere.[16,19,20]

Atomic Force Microscopy. Two substrates that have two different types of nanopatterns were chosen for the cell culture study. $PS_{610}P4VP_{130}$ generated lamellar domains (LS1) or wormlike nanopatterns while $PS_{1350}P2VP_{400}$ generated, on the other hand, cylindrical domains (DS1) or dotlike nanopatterns (Figure 1). Uncoated mica substrates (PM) were used as controls in the study.

The nanopatterns could be obtained with good reproducibility; more than 80% of the coated substrates had consistent nanostructures. Table 1 displays the physical properties of the nanopatterns generated by DS1 and LS1. DS1 substrates had dotlike structures of an average height and average surface roughness of 6.0 ± 0.5 nm (n = 6) and 0.47 ± 0.07 nm (n = 4), respectively, while those of LS1 substrates were 3.2 ± 0.2 nm (n = 5) and 0.17 ± 0.02 nm (n = 5), respectively. Dotlike structures on DS1 substrates had an average diameter of 200 ± 10 nm, with a center−center spacing of 290 ± 20 nm (n = 4). Wormlike structures on LS1 substrates had an average width of 160 ± 7 nm (n = 10). The surface of DS1 substrates was occupied 21.3 ± 1.5% (n = 7) by the hydrophobic PS aggregates while 61.1 ± 1.9% (n = 8) of the surface of LS1 was covered by the PS aggregates.

Prior to culturing cells on the substrates, the stability of the nanopatterns under culture conditions was investigated via AFM in both tapping mode (in air) and contact mode using a liquid cell filled with phosphate-buffered solution (PBS). Substrates were analyzed after subjecting them to sterilization with 70%

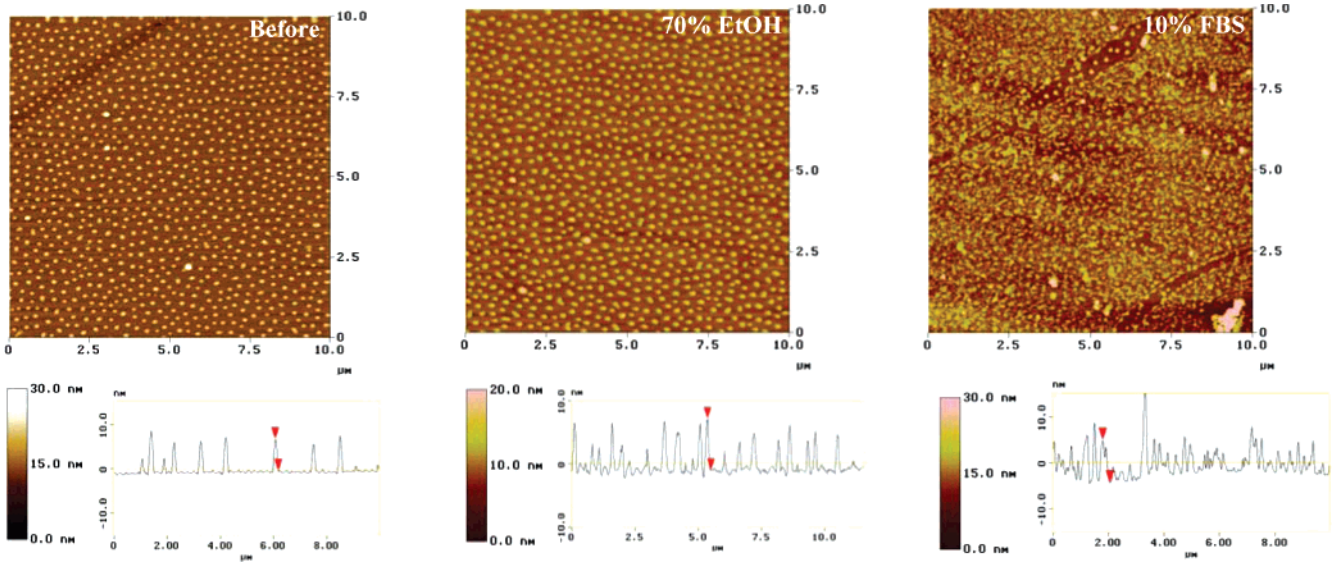

Figure 3. AFM images of the original DS1 substrates and of the substrates after sterilization with 70% ethanol and after incubation with cell culture medium supplemented with 10% FBS. DS1 substrate after incubation with cell culture medium supplemented with 10% FBS shown here was scanned in PBS in the contact mode. (The cross-sectional profile of the substrate along a straight line picked at random is shown at the bottom right of each AFM image.)

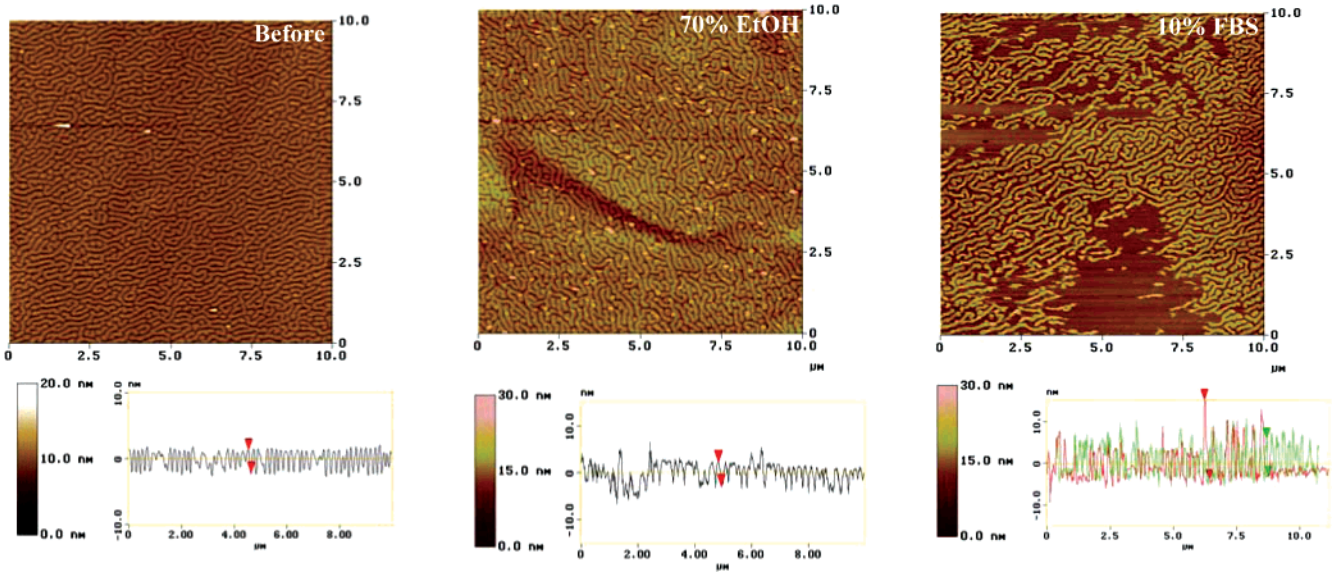

Figure 4. AFM images of the original LS1 substrates and of the substrates again after sterilization with 70% ethanol and after incubation with cell culture medium supplemented with 10% FBS. LS1 substrate after incubation with cell culture medium supplemented with 10% FBS shown here was scanned in PBS in the contact mode. (The cross-sectional profile of the substrate along a straight line picked at random is shown at the bottom right of each AFM image.)

ethanol and incubation in cell culture medium (37 °C for 2 h). Randomly dispersed aggregates of serum proteins were adsorbed on the surface of uncoated mica substrates generating a heterogeneous topography with heights up to 7.5 nm and surface roughness of about 0.28 nm (Figure 2). The nanopatterns were not affected by sterilization with 70% ethanol (Figures 3 and 4). Scanning in phosphate-buffered solution (PBS) (contact mode) showed that the nanopatterns remained in the original configuration after incubating 2 h with cell culture medium (Figures 3 and 4). Some parts of the SINPAT were seen to be removed by the AFM tip when scanning in the contact mode (Figure 4). In the tapping mode, no removal of the layer was seen (Figure 5). There was some reorientation of the SINPAT in both DS1 and LS1 substrates observed in Figure 5 which was due to swelling and contraction of the adsorped SINPAT layer after one cycle of incubation and drying the samples in the process of preparing them for the AFM analysis (tapping mode in air). The average surface roughness for the LS1 substrates after cell culture medium treatment was found to increase to 1.4 times that of the sterilized LS1 substrates, while the surface roughness for the DS1 substrates after cell culture medium treatment was found to be similar, decreasing slightly to 0.9 times that of the sterilized DS1 substrates. The substrates arranged in order of increasing surface roughness after incubating in medium supplemented with 10% FBS are PM $\ll$ LS1 $<$ DS1.

Contact Angle Measurement. Similar contact angle measurements from both the left and right sides of the sessile drop were recorded for all samples (Figure 6) showing that the surfaces were homogeneous for all substrates. The LS1 substrates had initially the most hydrophobic surfaces (99.7° $\pm$ 6.7°) because larger areas of the substrate surfaces were occupied by the more hydrophobic PS domains as shown earlier while DS1 substrates were expectantly more hydrophilic with contact angles of 44.2°

CDV

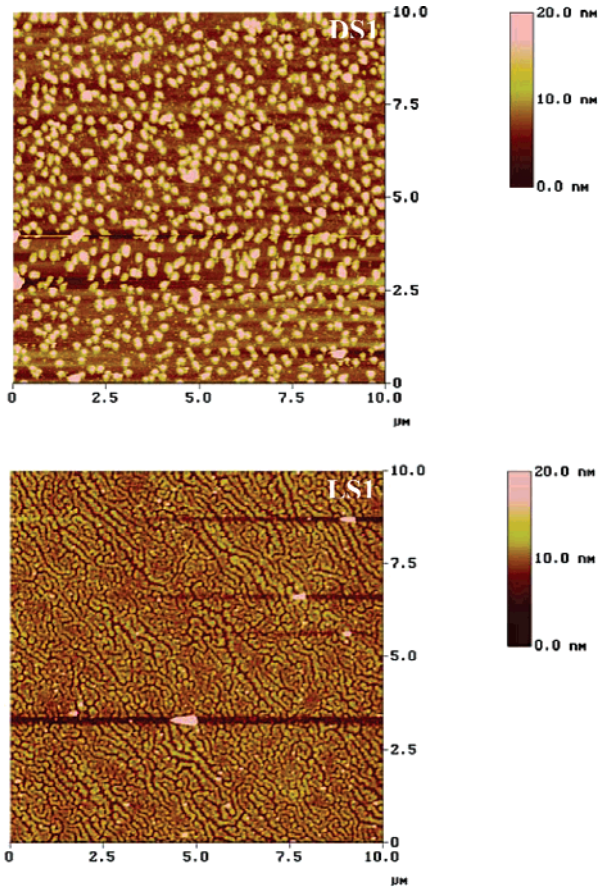

Figure 5. AFM images of DS1 and LS1 substrates after incubation with cell culture medium supplemented with 10% FBS which were scanned in the tapping mode.

± 1.3° (Figure 6). Both groups of substrates became more hydrophilic after sterilization with ethanol and had similar contact angles (66−70°) after cell culture medium (10% FBS) treatment although the surface of the DS1 substrates was initially much more hydrophilic (44.2° ± 1.3°). There was no change in contact angle of the DS1 substrates when they were incubated in medium with a lower FBS content (0.5% FBS). Contact angle of 66.5° ± 1.4° was measured on DS1 substrate incubated in 0.5% FBS supplemented medium, and contact angle of 67.0° ± 3.4° was measured on those incubated in 10% supplemented medium. Contact angle measurements showed that serum proteins were similarly adsorbed on both DS1 and LS1 substrates, but AFM data showed that the distinct topography of both substrates was still retained (Figures 3 and 4). Serum protein adsorption on the DS1 substrates reached saturation with only 0.5% FBS supplemented medium probably because of lesser available surface area for the dominant protein−substrate interaction which was between hydrophobic PS domains and the proteins. As expected, untreated non-SINPAT coated mica (PM) substrates were more hydrophilic ($<10^0$) compared to the other two groups of substrates, and the overall loading of serum proteins on PM substrates was lower than for DS1 and LS1 substrates. Cell culture studies on DS1 and LS1 substrates could be thus related to topographical influences since both substrates were treated in similar ways and had similar contact angle measurements after incubating in medium that was supplemented with 10% FBS for 2 h.

Cell Culture Studies. As shown previously, the SINPAT were found to be stable for both DS1 and LS1 substrates under cell culture conditions. A comparative cell culture study was done on three substrates, namely, plain mica (PM, control),

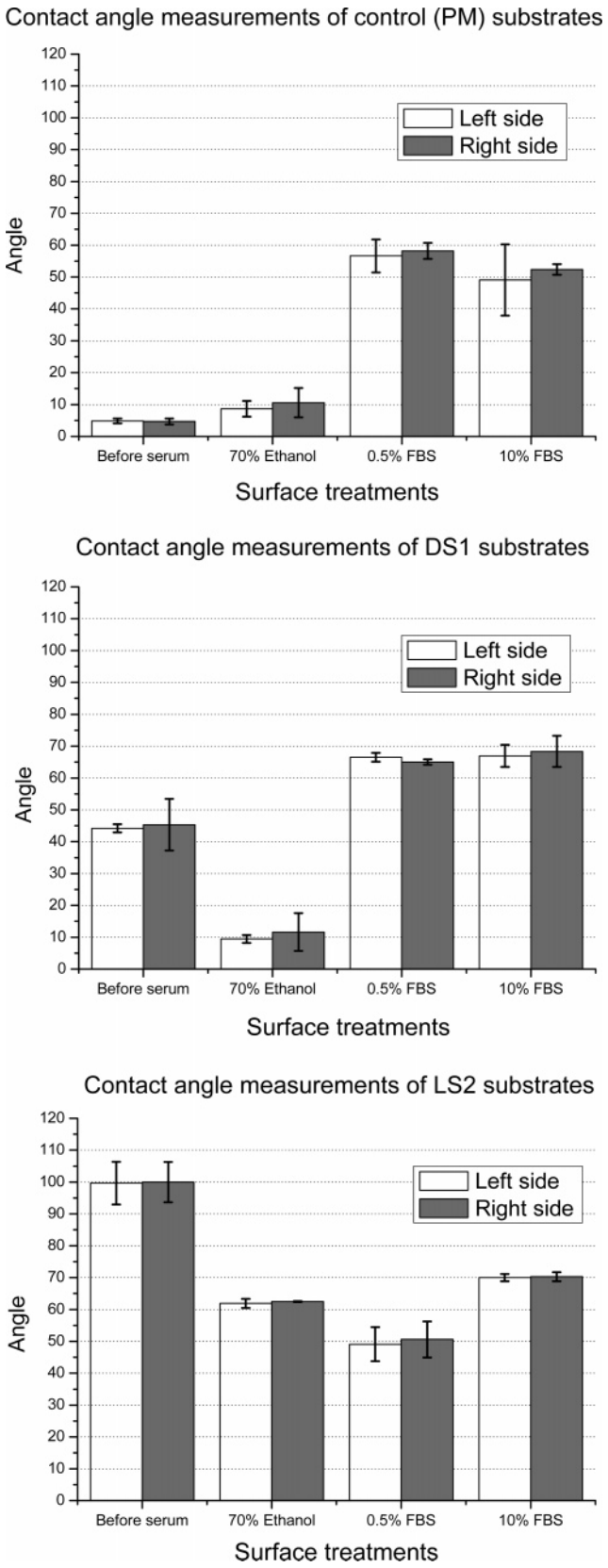

Figure 6. Contact angle measurements from both the left and right sides of the sessile drop were recorded for all samples treated after sterilization with ethanol and under cell culture conditions.

PS_{1350}-*b*-$P2VP_{400}$ coated mica (DS1) which had dot nanopatterns of average 200 ± 10 nm in diameter, and PS_{610}-*b*-$P4VP_{130}$ (LS1) coated mica which had lamellar nanopatterns with an average width of 160 ± 7 nm to examine the influence of distinctly shaped nanopatterns on cell behavior.

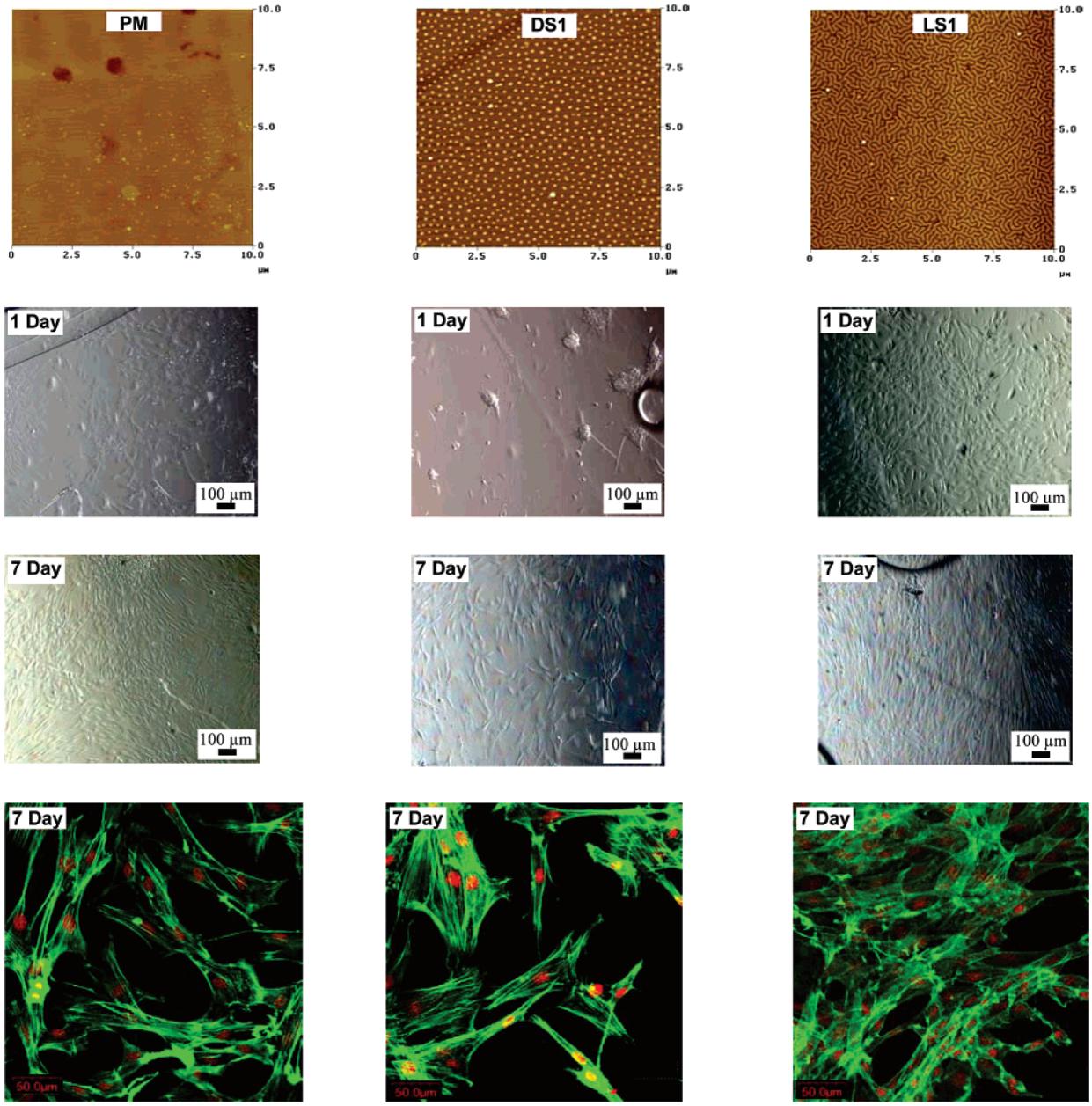

Figure 7. Microscopic images correspond to fibroblast culture on the respective substrates at the top of each column. Light microscopy pictures taken at day 1 and 7 are shown in the middle. Confocal laser microscopic images are at the end of each column. Confocal images showed cells stained with phalloidin (actin filaments, green) and propidium iodide (nucleus, red). LS1 substrates promoted earlier fibroblasts adhesion and enhanced proliferation.

Dermal Fibroblasts. All substrates were sterilized with 70% ethanol prior to seeding. On the first day postseeding, fibroblasts on all groups of substrates displayed the typical dipolar morphology (Figure 7). LS1 substrates promoted earlier fibroblast adhesion and higher fibroblast proliferation when compared to DS1 and PM substrates. A confluent monolayer of fibroblasts was observed on LS1 substrates after 7 days in vitro. DS1 substrates showed the least confluent cell population after 7 days of culture.

For the control substrates (PM substrates), fibroblasts population appeared to be denser than on DS1 but less dense than on LS1 on the first day postseeding (Figure 7). Generally, the nuclei of the fibroblasts on PM substrates were more prominent compared to the other two groups of substrates at day 1 (Figure 7). Fibroblasts were more flattened on the PM substrates than on the DS1 and LS1 surfaces. A monolayer of fibroblasts was observed on the PM substrates after 7 days in vitro in which fibroblasts proliferated in more than one direction.

In contrast, on the first day postseeding, cell aggregates attached on the DS1 substrates from which fibroblasts were migrating (Figure 7). These fibroblastic nodules indicated that the fibroblasts were under stressed conditions in this cell culture environment. The space between the nodules was sparsely populated with cells. Fibroblasts on LS1 substrates generally displayed more prominent spindle-shape morphology on the first day after seeding. They had more bulging cell bodies and thin elongated cytoplasmic ends. Cell layers in large areas of the LS1 substrates were mostly unidirectional after 7 days in vitro. Contact inhibition influenced cell morphology once cell confluency was reached.

In general, as the culture matured, it was observed by confocal laser microscopy that fibroblasts in the DS1 group of substrates had longer cytoplasmic extensions or filopodia. F-actin filaments extended throughout the cell. Microspikes were observed at the elongated filopodia of the migrating fibroblasts. The dotlike nanostructures of 200 ± 10 nm diameter with heights of 6.0 ±

CDV

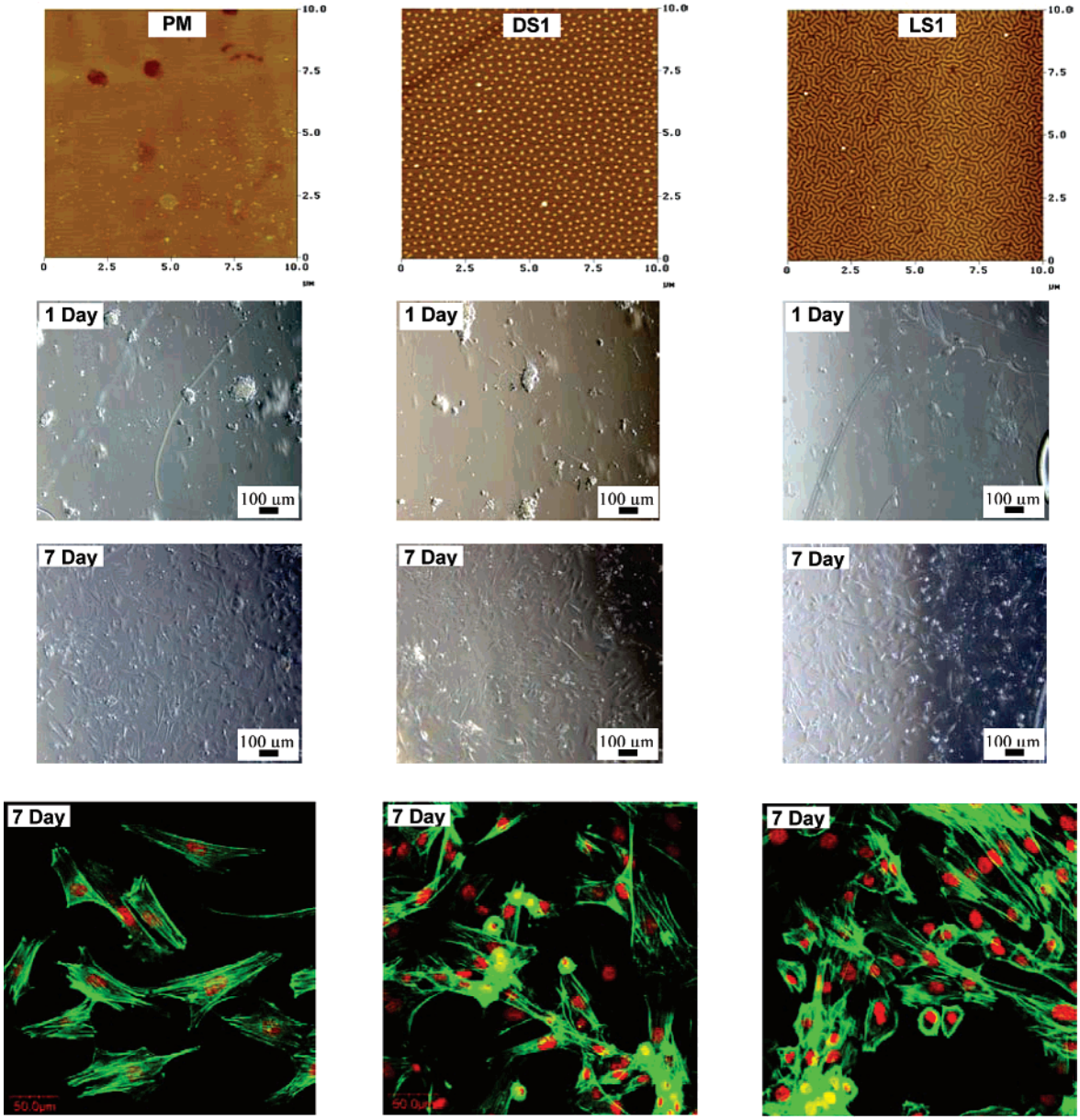

Figure 8. Microscopic images correspond to MPC cultures on the respective substrates at the top of each column. Phalloidin−PI staining (green−red) were observed under confocal laser microscopy. MPC culture on LS1 substrates is more confluent than the other two groups of substrates.

0.5 nm seemed to induce the fibroblasts to send out more filopodia to sense the environment surrounding them. In contrast, fibroblasts on PM substrates formed wider lamellipodia than those on DS1 substrates (Figure 7). After 7 days in vitro, multilayers of cells with prominently stained actin filaments were observed (Figure 7) on LS1 substrates which was in line with the optical microscope observations.

Mesenchymal Precursor Cells (MPC). MPC which also have a bipolar morphology were seeded on PM, DS1, and LS1 substrates (Figure 8). Cell aggregates were formed on all substrates after the first day postseeding. There were in general more single MPC and cell aggregate formations attached on the LS1 substrates. PM substrates were the least favorable for initial cell adhesion as cell aggregates were observed to be the least attached. The cell aggregates in the PM group of substrates were observed to move slightly in medium when the culture plates were tapped gently on day 1. Cell aggregates adhered better on DS1 substrates than on PM substrates though there were fewer single MPC on DS1 after first day postseeding. After 7 days postseeding, the MPC culture on LS1 substrates was slightly more confluent than the other two groups of substrates.

Phalloidin-PI stained cells showed some general differences in cell morphology between the three groups of substrates after 7 days postseeding (Figure 8). No distinct differences in cell sizes were observed in the three groups. MPC on PM substrates were generally more batlike in shape with migratory fronts on several faces of the cells exploring the relatively flat surface of non-SINPAT mica (confocal laser images in Figure 8). Distinct and thick actin bundles can be seen stretching through the MPC even right to the cell periphery.

MPC cultured on DS1 substrates had a more flattened morphology with the cells displaying a more cuboidal cell body compared to those on LS1 substrates. MPC on DS1 substrates had diffused actin filaments, gel-like network of actin bundles extending throughout the cell. Distinct actin bundles intersperse the MPC cell bodies, ending shortly before their cell periphery. More cells on DS1 substrates had a wider lamellipodia front ending in punctuate points than on LS1 substrates. Lower density

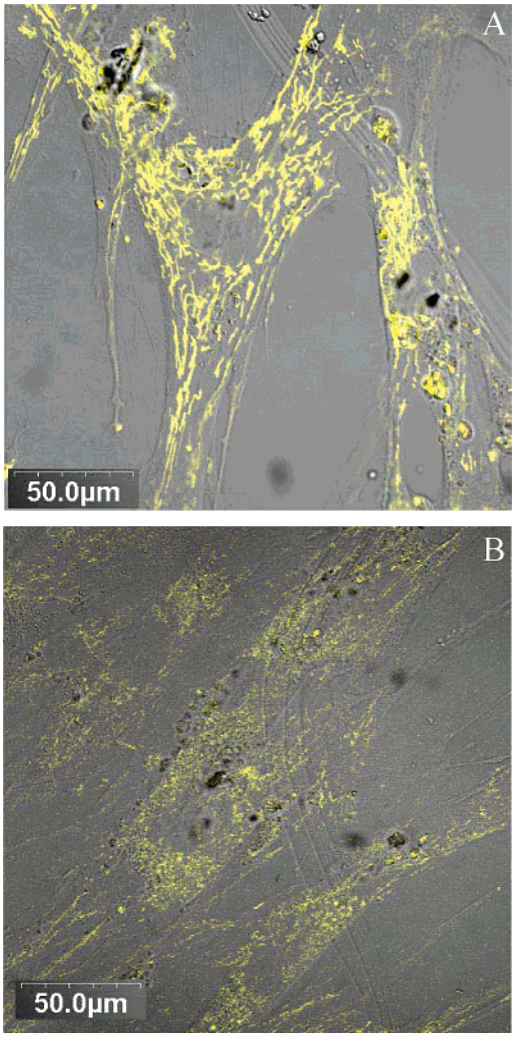

Figure 9. Confocal laser microscope images of transfected MPC expressing eYFP-α-tubulin (yellow) cultured on DS1 substrates (A) and LS1 substrates (B) after 5 days postseeding.

of actin bundles was present when compared to fibroblasts cultured on PM and LS1 substrates.

MPC cultured on LS1 substrates had denser, thicker actin bundles that were arranged in parallel fashion. They had also more elongated cell bodies compared to those on DS1 substrates, perhaps following the contours of the wormlike topography of LS1 substrates.

The MPC grown on DS1 and LS1 substrates had different microtubule arrangements (Figure 9). Microtubules could be observed as distinct, thick, and short fibers oriented in the direction of cell polarization in MPC cultured on DS1 substrates (Figure 9A). Short microtubules could be observed to polymerize to the MPC periphery on DS1 substrates. The microtubules in MPC grown on LS1 substrates were diffused and indistinct (Figure 9B). Long thin microtubules could be seen stretching from the polarized ends of the MPC on LS1 substrates.

AFM images of an adhered MPC on DS1 substrates showed a large and flattened lamellipodium with short microspikes (Figure 10). There were prominent and larger round adhesion sites on the upper surface of the cell. Comparatively, the lamellipodium of MPC on LS1 substrates was prominent with dense actin filaments and longer microspike extension in agreement with phalloidin-PI stained confocal laser images from Figure 8. The adhesion sites of MPC on LS1 appeared to be much smaller. The extracellular environment of the cells was also distinctly different.

As cells proliferated and migrated over the surfaces of substrata, they modified the extracellular matrix and left parts of their membrane behind. These external signals influence adhesion and motility of cells which in turn have effects on downstream signaling events within the cells. It could be observed on the atomic force micrographs (Figure 10) that the regions next to the cells on DS1 and LS1 substrates were distinctly different although the same type of cell was cultured on both substrates. The dotlike topography of the DS1 substrates could still be discerned after 7 days in culture. The extracellular matrix environment of the DS1 substrates appeared to mimic the original topography, with dotlike topography of up to 30 nm in height whereas the wormlike topography of the LS1 substrates was no longer distinct (Figure 10) because of a thicker layer of proteins. Extracellular matrix on the LS1 substrates had enlarged aggregates and densely packed elongated formations.

Discussion

Various techniques are now available to fabricate nanoscale features with control such as electron beam lithography,[21,22] photolithography,[23,24] and colloidal lithography.[11,12] Several of these methods involved a considerable amount of effort to produce nanoscale features and many produced nanopatterns that were inhomogeneous and randomly distributed. Surface-induced nanopattern formed by ultrathin diblock copolymer PS−PVP films are capable of having long-range order and can be easily controlled by varying the block length ratio of the diblock polymeric system.[20]

Ultrathin films of a poly(styrene)-*block*-poly(2-vinylpyrindine) diblock copolymer (PS-*b*-P2VP) and poly(styrene)-*block*-poly(4-vinylpyrindine) diblock copolymer (PS-*b*-P4VP) were used to form highly reproducible surfaced-induced nanopattern (SINPAT) on mica. Although the overall morphology of the films remained unchanged during the sterilization process, which indicated that no significant miscibility is induced during sterilization with 70% ethanol, we observed a significant reduction in contact angles in both DS1 and LS1 substrates. Elbs et al.[25] reported that a short treatment with a selective vapor and subsequent drying led to changes in the surface morphology. They reported that on drying the lower solubility phase will solidify first while the higher solubility phase will still be able to shrink. They found that the lower solubility phase protruded over the polymer layer with a higher solubility. PVP microdomains in our system would have a higher solubility in the 70% ethanol/water mixture than the PS microdomains, resulting in a reorientation of the PVP microdomains to the outside of the ultrathin film as the film dries. PS microdomains with a lower solubility will still aggregate over the PVP microdomains. Because we did not dry the coated substrates under vacuum condition after ethanol treatment, the PVP microdomains of PS-*b*-PVP polymer layer did not collapse to the original condition, and the hydrophilicity of both the DS1 and LS1 substrates subsequently increased.

We have shown that the nanopatterns formed were reproducible and stable under standard cell culture conditions. Moreover, the proliferation of the two cell types also appeared to show no correlation to the substrate surface roughness.

The formation of adhesion foci on suitable material surfaces occurs within minutes in a cell.[26,27] Signaling events generated between cells and material surfaces are triggered by integrins located in focal contacts formed by cells.[28,29] The cytoskeleton, linked to the integrins, is strongly associated with signal transductions. Molecular triggers have been found to relay from

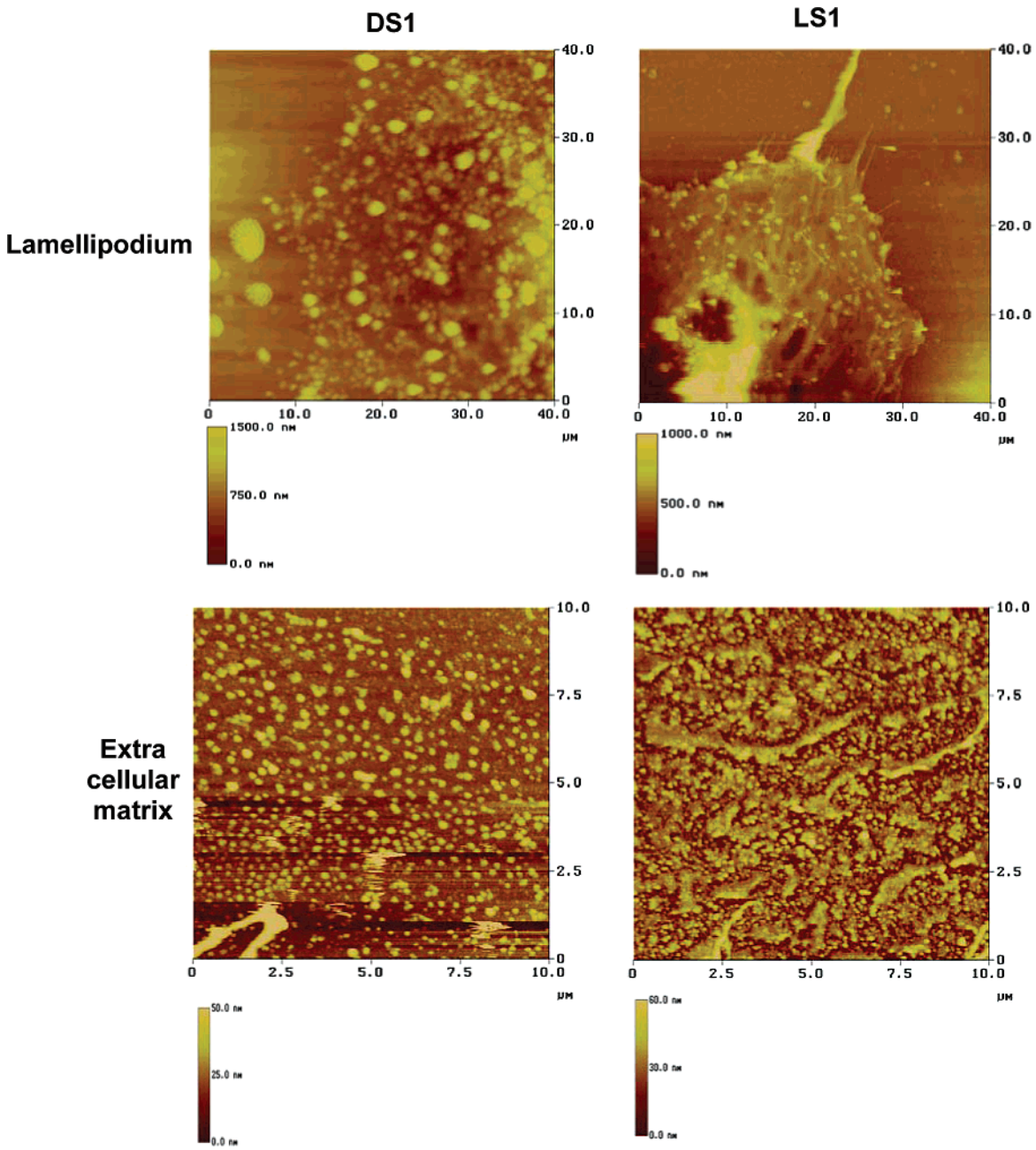

Figure 10. AFM images of the lamellipodia of MPC and the extracellular matrix next to the corresponding cells on DS1 and LS1 substrates after 7 days in vitro.

a cell's exterior to its interior via kinases.[30] These in turn regulate a plethora of downstream events such as cell division, differentiation, and cell migration. The process of polarization and cell motility of substrate-bound cells can be viewed as a competition between the motile compartment of the actin cytoskeleton, comprised of lamellipodia and filopodia, and the anchorage compartment, comprised of stress fiber bundles and focal adhesions.

Fibroblasts and MPC had been shown to react to topographies as small as 10 nm.[11,12,31] It was found in this study that fibroblasts and MPC were adhering and therefore proliferating better on nanofeatures that were wormlike than dotlike. Dalby et al.[13] found that fibroblasts had well-formed focal adhesions on smooth surfaces compared to surfaces with nanocolumns of height 160 nm and diameter 100 nm. This could be because fibroblasts formed dot adhesions that were transient in nature.[32] We discovered that fibroblasts were better attached to flat surfaces compared to dotlike substrates and our findings are in line with what Dalby et al.[13] observed. Fibroblasts produced more filopodia which are involved in chemical and topograhical sensing[33] on the dotlike substrates. The fibroblasts seemed to be sending out more filopodia to sense their surroundings perhaps trying to find more anchor points on the dotlike substrates (DS1).

MPC are multipotent cells capable of differentiating into different lineages of mesenchymal tissues, including bone,[34] and could be cultured in scaffolds for applications as bone substitutes.[35] It is, therefore, of interest to study the response of MPC on the nanopatterns to allow better adhesion and in turn faster proliferation on the scaffolds before differentiating them. Dalby et al.[12] showed that MPC were able to respond to nanostructures and express extracellular osteogenic proteins compared to smooth surfaces. Similarly in our study, MPC prefered a topography with nanopatterns to smooth surfaces (PM), proliferating best on the wormlike structures.

It has been reported recently that the size of integrin in the cell membrane is between 8 and 12 nm.[36] Walter et al.[14] and Calvalcanti-Adam et al.[36] investigated the relationship between varying the distances between gold nanoparticles functionalized with an integrin-specific ligand and cellular adhesion. The gold nanoparticles were of diameter of 6 nm each which binds to one integrin and were distanced from between 58 and 145 nm. They found that rat fibroblasts were better attached to functionalized nanopatterns that were closely spaced together (58 nm). Although serum proteins, namely, fibronectin and vitronectin, were adsorped to a similar extent on both DS1 and LS1 substrates as observed by the similar contact angles after incubation with 10% FBS supplemented media, both cell types showed a trend of improved proliferation and adhesion on wormlike substrate (LS1). This could be due to the shorter distances between the adsorped proteins on the LS1 substrates than on the DS1 substrates because of the closely packed PS domains to which the proteins adsorped.

Microtubules exert their influence on cell polarization by modulating adhesion site turnover.[26,27] It has been observed that microtubule ends invaded vinculin positive contact sites in fibroblast lamellipodia.[26] At regions of high adhesion site turnover such as at the lamellipodia, there is increased microtubule targeting as the cell moves. It has been shown that if there is a block in microtubule organization it will result in large adhesion sites. Microtubule stability is dependent on a stressed actin cytoskeleton. MPC on DS1 had thick and short microtubule fibers that could be seen at the cell periphery too. A diffused actin network right up to the cell periphery in MPC on DS1 substrates could ensure stability of microtubules up to the cell periphery as observed in Figure 9. Cytoskeleton consisting of short microtubules could perhaps result in a much localized adhesion site turnover resulting in larger adhesion sites such as those observed in Figure 10. Larger adhesion sites could be an indication that MPC were not as motile on the DS1 substrates. A diffuse microtubule network in MPC on LS1 substrates on the other hand could result in a higher turnover of adhesion sites resulting in smaller adhesion sites as observed in Figure 10. MPC on LS1 substrates were elongated with dense parallel actin bundles putting themselves in high tension perhaps allowing the microtubules to distribute homogenously thoughout the cells.

Another effect of the different nanopatterns could be observed in the way the cells modify their extracellular environment as they migrate over the surface. As cells migrate over the nanopatterns, they deposit extracellular matrix proteins and leave bits of their plasma membrane behind, remodeling their extracellular matrix. The extracellular matrix was distinctly different on both substrates after 7 days of cell culture. It appeared to be conforming to the nanotopography of the surfaces as the dotlike pattern of DS1 could still be observed after 7 days of cell culture while elongated protein aggregates were found on LS1 substrates mimicking the underlying topography. Proteins passively adsorb to polystyrene surfaces through hydrophobic interactions. Approximately 3 times the area of LS1 substrates was occupied by the polystyrene aggregates compared to that of DS1 allowing the formation of a thicker layer of proteins on LS1.

Conclusions

The different nanopatterns of heights less than 10 nm appeared to elicit different rates of adhesion and proliferation in fibroblasts and mesenchymal precursor cells. Although the surface energy of the SINPAT substrates was similar after cell culture medium treatment, the cells remodeled the extracellular matrix environment differently during their migration. Dermal fibroblasts and mesenchymal precursor cells were observed to prefer the $PS_{610}P4VP_{130}$ (wormlike) coated substrate. By discovering the type of topography that each cell type preferentially grows on, we can create textured biomaterials to selectively propagate a particular cell type and optimize cellular adhesion and proliferation.

Acknowledgment. This work was supported by the Science and Research Council, Singapore, under Grant Number MCE/TP/00/001.2 D. W. Hutmacher acknowledges the support of the National University of Singapore (NUS Young Investigator Grant WBS 397 000 003 650).

References and Notes

(1) Wilson, C. J.; Clegg, R. E.; Leavesley, D. I.; Pearcy, M. J. Mediation of biomaterial-cell interactions by adsorbed proteins: A review [Review]. *Tissue Eng.* **2005**, *11* (1−2), 1−18.
(2) Goodman, S. L.; Sims, P. A.; Albrecht, R. M. Three-dimensional extracellular matrix textured biomaterials. *Biomaterials* **1996**, *17* (21), 2087−2095.
(3) Curtis, A.; Wilkinson, C. Topographical control of cells [Review]. *Biomaterials* **1997**, *18* (24), 1573−1583.
(4) Flemming, R. G.; Murphy, C. J.; Abrams, G. A.; Goodman, S. L.; Nealey, P. F. Effects of synthetic micro- and nano-structured surfaces on cell behavior [Review]. *Biomaterials* **1999**, *20* (6), 573−588.
(5) Clark, P.; Connolly, P.; Curtis, A. S.; Dow, J. A.; Wilkinson, C. D. Topographical control of cell behaviour: II. Multiple grooved substrata. *Development* **1990**, *108* (4), 635−44.
(6) Clark, P.; Connolly, P.; Curtis, A. S.; Dow, J. A.; Wilkinson, C. D. Cell guidance by ultrafine topography in vitro. *J. Cell Sci.* **1991**, *99* (Pt 1), 73−7.
(7) Wojciak-Stothard, B.; Curtis, A.; Monaghan, W.; MacDonald, K.; Wilkinson, C. Guidance and activation of murine macrophages by nanometric scale topography. *Exp. Cell Res.* **1996**, *223* (2), 426−35.
(8) Hamilton, D. W.; Riehle, M. O.; Monaghan, W.; Curtis, A. S. Articular chondrocyte passage number: influence on adhesion, migration, cytoskeletal organisation and phenotype in response to nano- and micro-metric topography. *Cell Biol. Int.* **2005**, *29* (6), 408−21.
(9) Yim, E. K. F.; Reano, R. M.; Pang, S. W.; Yee, A. F.; Chen, C. S.; Leong, K. W. Nanopattern-induced changes in morphology and motility of smooth muscle cells. *Biomaterials* **2005**, *26* (26), 5405−5413.
(10) Andersson, A. S.; Backhed, F.; von Euler, A.; Richter-Dahlfors, A.; Sutherland, D.; Kasemo, B. Nanoscale features influence epithelial cell morphology and cytokine production. *Biomaterials* **2003**, *24* (20), 3427−3436.
(11) Dalby, M. J.; Riehle, M. O.; Sutherland, D. S.; Agheli, H.; Curtis, A. S. G. Fibroblast response to a controlled nanoenvironment produced by colloidal lithography. *J. Biomed. Mater. Res., Part A* **2004**, *69A* (2), 314−322.
(12) Dalby, M. J.; McCloy, D.; Robertson, M.; Agheli, H.; Sutherland, D.; Affrossman, S.; Oreffo, R. O. C. Osteoprogenitor response to semi-ordered and random nanotopographies. *Biomaterials* **2006**, *27* (15), 2980−2987.
(13) Dalby, M. J.; McCloy, D.; Robertson, M.; Wilkinson, C. D. W.; Oreffo, R. O. C. Osteoprogenitor response to defined topographies with nanoscale depths. *Biomaterials* **2006**, *27* (8), 1306−1315.
(14) Walter, N.; Selhuber, C.; Kessler, H.; Spatz, J. P. Cellular unbinding forces of initial adhesion processes on nanopatterned surfaces probed with magnetic tweezers. *Nano Lett.* **2006**, *6* (3), 398−402.
(15) Wojciak, B.; Crossan, J.; Curtis, A. S. G.; Wilkinson, C. D. W. Grooved substrata facilitate in vitro healing of completely divided flexor tendons. *J. Mater. Sci.: Mater. Med.* **1995**, *6* (5), 266−271.
(16) Spatz, J. P.; Eibeck, P.; Mossmer, S.; Moller, M.; Kramarenko, E. Y.; Khalatur, P. G.; Potemkin, I. I.; Khokhlov, A. R.; Winkler, R. G.; Reineker, P. Order-disorder transition in surface-induced nanopattern of diblock copolymer films. *Macromolecules* **2000**, *33* (1), 150−157.
(17) Spatz, J. P.; Moller, M.; Noeske, M.; Behm, R. J.; Pietralla, M. Nanomosaic surfaces by lateral phase separation of a diblock copolymer. *Macromolecules* **1997**, *30* (13), 3874−3880.

(18) Spatz, J. P.; Sheiko, S.; Moller, M. Substrate-induced lateral microphase separation of a diblock copolymer. *Adv. Mater.* **1996**, *8* (6), 513 ff.
(19) Eibeck, P.; Spatz, J. P.; Potemkin, I.; Kramarenko, E. Y.; Khokhlov, A. R.; Moller, M. Molecular weight dependent structural transitions in surface-induced nanopatterns of ultrathin films of poly(styrene)-block-poly(vinylpyridine) on mica. In *Abstracts of Papers of the 218th Meeting of the American Chemical Society, Part 2*, Aug 22, 1999; American Chemical Society: Washington, DC, 1999; pp U507.
(20) Potemkin, I. I.; Kramarenko, E. Y.; Khokhlov, A. R.; Winkler, R. G.; Reineker, P.; Eibeck, P.; Spatz, J. P.; Moller, M. Nanopattern of diblock copolymers selectively adsorbed on a plane surface. *Langmuir* **1999**, *15* (21), 7290−7298.
(21) Cumming, D. R. S.; Thoms, S.; Beaumont, S. P.; Weaver, J. M. R. Fabrication of 3 nm wires using 100 Kev electron beam lithography and poly(methyl methacrylate) resist. *Appl. Phys. Lett.* **1996**, *68* (3), 322−324.
(22) Vieu, C.; Carcenac, F.; Pepin, A.; Chen, Y.; Mejias, M.; Lebib, A.; Manin-Ferlazzo, L.; Couraud, L.; Launois, H. Electron beam lithography: resolution limits and applications. *Appl. Surf. Sci.* **2000**, *164*, 111−117.
(23) Curtis, A. S.; Casey, B.; Gallagher, J. O.; Pasqui, D.; Wood, M. A.; Wilkinson, C. D. Substratum nanotopography and the adhesion of biological cells. Are symmetry or regularity of nanotopography important? *Biophys. Chem.* **2001**, *94* (3), 275−83.
(24) Wilkinson, C. D. W.; Riehle, M.; Wood, M.; Gallagher, J.; Curtis, A. S. G. The use of materials patterned on a nano- and micro-metric scale in cellular engineering. *Mater. Sci. Eng.* 19, (1−2 Special Issue SI), Biomimetic Materials.
(25) Elbs, H.; Fukunaga, K.; Stadler, R.; Sauer, G.; Magerle, R.; Krausch, G. Microdomain morphology of thin ABC triblock copolymer films. *Macromolecules* **1999**, *32* (4), 1204−1211.
(26) Kaverina, I.; Krylyshkina, O.; Small, J. V. Microtubule targeting of substrate contacts promotes their relaxation and dissociation. *J. Cell Biol.* **1999**, *146* (5), 1033−1043.
(27) Kaverina, I.; Krylyshkina, O.; Small, J. V. Regulation of substrate adhesion dynamics during cell motility [Review]. *Int. J. Biochem. Cell Biol.* **2002**, *34* (7), 746−761.
(28) Juliano, R. L.; Haskill, S. Signal transduction from the extracellular matrix. *J. Cell Biol.* **1993**, *120* (3), 577−85.
(29) Reiske, H. R.; Kao, S. C.; Cary, L. A.; Guan, J. L.; Lai, J. F.; Chen, H. C. Requirement of phosphatidylinositol 3-kinase in focal adhesion kinase-promoted cell migration. *J. Biol. Chem.* **1999**, *274* (18), 12361−6.
(30) Cary, L. A.; Cooper, J. A. Molecular switches in lipid rafts. [comment]. *Nature* **2000**, *404* (6781), 945.
(31) Dalby, M. J.; Riehle, M. O.; Johnstone, H. J. H.; Affrossman, S.; Curtis, A. S. G. Nonadhesive nanotopography: Fibroblast, response to poly(n-butyl methacrylate)-poly(styrene) demixed surface features. *J. Biomed. Mater. Res., Part A* **2003**, *67A* (3), 1025−1032.
(32) Bershadsky, A. D.; Tint, I. S.; Neyfakh, A. A., Jr.; Vasiliev, J. M. Focal contacts of normal and RSV-transformed quail cells. Hypothesis of the transformation-induced deficient maturation of focal contacts. *Exp. Cell Res.* **1985**, *158* (2), 433−44.
(33) Wood, W.; Martin, P. Structures in focus - filopodia. *Int. J. Biochem. Cell Biol.* **2002**, *34* (7), 726−730.
(34) Pittenger, M. F.; Mackay, A. M.; Beck, S. C.; Jaiswal, R. K.; Douglas, R.; Mosca, J. D.; Moorman, M. A.; Simonetti, D. W.; Craig, S.; Marshak, D. R. Multilineage potential of adult human mesenchymal stem cells. *Science* **1999**, *284* (5411), 143−7.
(35) Endres, M.; Hutmacher, D. W.; Salgado, A. J.; Kaps, C.; Ringe, J.; Reis, R. L.; Sittinger, M.; Brandwood, A.; Schantz, J. T. Osteogenic induction of human bone marrow-derived mesenchymal progenitor cells in novel synthetic polymer-hydrogel matrices. *Tissue Eng.* **2003**, *9* (4), 689−702.
(36) Cavalcanti-Adam, E. A.; Micoulet, A.; Blummel, J.; Auernheimer, J.; Kessler, H.; Spatz, J. P. Lateral spacing of integrin ligands influences cell spreading and focal adhesion assembly. *Eur. J. Cell Biol.* **2006**, *85* (3−4), 219−224.

BM0611533